Astronomy & Astrophysics manuscript no. mignoli
February 2, 2022
© ESO 2022

arXiv:0810.2245v1 [astro-ph] 13 Oct 2008

The zCOSMOS redshift survey: the three-dimensional classification cube and bimodality in galaxy physical properties ⋆

M. Mignoli[1], G. Zamorani[1], M. Scodeggio[2], A. Cimatti[3], C. Halliday[4] ⋆⋆, S.J. Lilly[5], L. Pozzetti[1], D. Vergani[1,2], C. M. Carollo[5], T. Contini[6], O. Le Févre[7], V. Mainieri[8], A. Renzini[9], S. Bardelli[1], M. Bolzonella[1], A. Bongiorno[10], K. Caputi[5], G. Coppa[3,1], O. Cucciati[11], S. de la Torre[7], L. de Ravel[7], P. Franzetti[2], B. Garilli[2], A. Iovino[11], P. Kampczyk[5], J.-P. Kneib[7], C. Knobel[5], K. Kovač[5], F. Lamareille[6,1], J.-F. Le Borgne[6], V. Le Brun[7], C. Maier[5], R. Pellò[6], Y. Peng[5], E. Perez Montero[6], E. Ricciardelli[9], C. Scarlata[5], J.D. Silverman[5,8], M. Tanaka[8], L. Tasca[7], L. Tresse[7], E. Zucca[1], U. Abbas[7], D. Bottini[2], P. Capak[12], A. Cappi[1], P. Cassata[7], M. Fumana[2], L. Guzzo[11], A. Leauthaud[7], D. Maccagni[2], C. Marinoni[13], H.J. McCracken[14], P. Memeo[2], B. Meneux[11], P. Oesch[5], C. Porciani[5], R. Scaramella[15], and N. Scoville[12]

[1] INAF – Osservatorio Astronomico di Bologna, Bologna, Italy
[2] INAF – Istituto di Astrofisica Spaziale e Fisica Cosmica, Milano, Italy
[3] Dipartimento di Astronomia, Università degli Studi di Bologna, Bologna, Italy
[4] INAF – Osservatorio Astronomico di Arcetri, Firenze, Italy
[5] Institute of Astronomy, ETH Zurich, Zurich, Switzerland
[6] Laboratoire d'Astrophysique de Toulouse-Tarbes, Université de Toulouse, CNRS Toulouse, France,
[7] Laboratoire d'Astrophysique de Marseille, Marseille, France
[8] European Southern Observatory, Garching, Germany
[9] Dipartimento di Astronomia, Università di Padova, Padova, Italy
[10] Max Planck Institut für Extraterrestrische Physik, Garching, Germany
[11] INAF – Osservatorio Astronomico di Brera, Milano, Italy
[12] California Institute of Technology, Pasadena, CA, USA
[13] Centre de Physique Theorique, Marseille, Marseille, France
[14] Institut d'Astrophysique de Paris, Université Pierre & Marie Curie, Paris, France
[15] INAF – Osservatorio Astronomico di Roma, Monte Porzio Catone , Italy

Received / Accepted

ABSTRACT

Aims. We investigate the relationships between three main optical galaxy observables (spectral properties, colours, and morphology), exploiting the data set provided by the COSMOS/zCOSMOS survey. The purpose of this paper is to define a simple galaxy classification cube, using a carefully selected sample of ≈ 1000 galaxies.
Methods. Using medium resolution spectra of the first 1*k* zCOSMOS-bright sample, optical photometry from the Subaru/COSMOS observations, and morphological measurements derived from ACS imaging, we analyze the properties of the galaxy population out to $z \sim 1$. Applying three straightforward classification schemes (spectral, photometric, and morphological), we identify two main galaxy types, which appear to be linked to the bimodality of galaxy population. The three parametric classifications constitute the axes of a "classification cube".
Results. A very good agreement exists between the classification from spectral data (quiescent/star-forming galaxies) and that based on colours (red/blue galaxies). The third parameter (morphology) is less well correlated with the first two: in fact a good correlation between the spectral classification and that based on morphological analysis (early-/late-type galaxies) is achieved only after partially complementing the morphological classification with additional colour information. Finally, analyzing the 3D-distribution of all galaxies in the sample, we find that about 85% of the galaxies show a fully concordant classification, being either quiescent, red, bulge-dominated galaxies (∼ 20%) or star-forming, blue, disk-dominated galaxies (∼ 65%). These results imply that the galaxy bimodality is a consistent behaviour both in morphology, colour and dominant stellar population, at least out to $z \sim 1$.

Key words. galaxies: general – galaxies: evolution – galaxies: fundamental parameters (classification)

⋆ Based on observations undertaken at the European Southern Observatory (ESO) Very Large Telescope (VLT) under Large Program 175.A-0839. Also based on observations with the NASA/ESA Hubble Space Telescope, obtained at the Space Telescope Science Institute, operated by AURA Inc., under NASA contract NAS 5-26555, with the Subaru Telescope, operated by the National Astronomical Observatory of Japan, with the telescopes of the National Optical Astronomy Observatory, operated by the Association of Universities for Research in Astronomy, Inc. (AURA) under cooperative agreement with the National Science Foundation, and with the Canada-France-Hawaii Telescope, operated by the National Research Council of Canada, the Centre National de la Recherche Scientifique de France and the University of Hawaii.

⋆⋆ *Present address:* Department of Physics and Astronomy, University of Glasgow, Glasgow G12 8QQ, United Kingdom

1. Introduction

Galaxies have a wide variety of physical and observational properties. However, since the early works of Humason (1936) and Hubble (1938) it has been known that the morphologies of galaxies correlate with their colours and consequently with the derived properties of their stellar population. Large efforts have been undertaken to establish reliable relationships between the morphological types, colours, and spectral characteristics of the galaxies (i.e. Fioc & Rocca-Volmerange, 1999; Bershady et al., 2000). The accurate determination of these relationships is of paramount importance to our understanding of galaxy formation and evolution. The main galaxy optical properties are the spectral energy distributions, spectral line properties, internal velocity dispersions, morphologies, sizes, and structural components. From these observable quantities, we can derive intrinsic physical properties, such as stellar and gaseous masses, metallicities, and star-formation histories; each of these aspects provides crucial clues about how galaxies were created and have evolved. The most basic evolutionary processes and their corresponding observables are, however, not yet clear and we are still uncertain whether the correlations between galaxy properties observed are driven by fundamental aspects of the galaxy population (Conselice, 2006). The goal of this paper is to investigate the relationships between the three main optical galaxy observables (spectral properties, colours, and morphology) by taking advantage of the unique data set provided by the COSMOS/zCOSMOS survey.

A fundamental property discovered by large surveys such as the Sloan Digital Sky Survey (SDSS) and the Two-Degree Field Galaxy Redshift Survey (2dFGRS), is that the optical colour distribution of galaxies at low redshift can be represented by a bimodal function (Strateva et al., 2001; Wild et al., 2005). The bimodality separates the locus of star-forming galaxies from that of early-type galaxies (ellipticals, $S0$, and early-type spirals), such that the fraction of the red, passive population increases progressively with the luminosity, becoming smaller than the blue fraction for $M_r > -20$ and dominating the distribution for $M_r < -21$ (Baldry et al., 2004). The bimodality is also present in different aspects of the galaxy population: structural parameters such as concentration index (Ball et al., 2006) and disk-to-bulge ratio (Drory & Fisher, 2007), and spectral features such as $D4000$ and line ratios (Kauffmann et al., 2003; Balogh et al., 2004a; Yan et al., 2006; Franzetti et al., 2007), all exhibit strong bimodal distributions. The bimodality in galaxy properties, clearly evident in the local Universe, is still present at $z \sim 1$ (Bell et al., 2004), but it is less clear whether the two distinct galaxy populations hold at higher redshifts (up to $z = 2$; Giallongo et al., 2005; Cirasuolo et al., 2007; Cassata et al., 2008). A key test for galaxy evolution models is to explain why this bimodality occurs; it is still unclear which processes produce two sets of galaxies of different average colours and dispersions and different luminosity ranges.

Determining the nature of the bimodality can be approached by means of large spectroscopic redshift surveys, studying the measured galaxy parameters as a function of redshift, luminosity, and spectral properties. The zCOSMOS survey opens the possibility to extend the study of bimodality out to $z \sim 1$.

zCOSMOS is a large redshift survey that is being undertaken in the COSMOS field as an ESO Large Programme (~ 600 hours of observation) with the VIMOS spectrograph at the VLT. The survey consists of two parts: the first part targets a magnitude-limited sample selected from ACS images to have $I_{AB} < 22.5$ and observed at medium resolution; this will provide spectra and redshifts for $\approx 20,000$ galaxies out to $z \sim 1.5$ over two square degrees. The second and deeper part of the survey is acquiring spectroscopy to measure the redshifts of $\approx 12,000$ galaxies at $1.4 < z < 2.5$ at lower resolution and over the central square degree, by selecting targets using various colour-selection criteria.

This paper, based mainly on the spectroscopic data of the zCOSMOS survey, takes advantage of the large potential of the COSMOS database. We present the analysis of a representative sample of the bright component of the full survey, consisting of around 1200 galaxies observed during the first year of observations. Using the medium resolution spectra of these objects and complementing them with the optical photometry from the COSMOS multi-band catalog (Capak et al., 2007) and morphological information derived from ACS imaging (Scoville et al., 2007; Scarlata et al., 2007a), we investigate the optical properties of the galaxy population out to $z \sim 1$. Applying three straightforward classifications (spectral, photometric, and morphological), we are able to distinguish two main galaxy types, which are intimately connected with the bimodality and formation history of the galaxy population: the three parametric classifications constitute the axes of a "classification cube". It is important to remark that we develop our cube using only observational parameters, such as emission-line equivalent widths, continuum indices, photometric colours (and not synthetic colours), and a non-parametric morphological classification. The choice is motivated by the desire to avoid dependence on models, galaxy templates, and parametrization of galaxy properties. Moreover, using simple observed properties makes the classification cube easy to replicate in other galaxy surveys.

The principal aim of this paper is the definition of the galaxy classification cube, using a fair but relatively small sample of ≈ 1000 galaxies. The full exploitation of the classification cube, applied to larger galaxy samples (i.e. the 10K zCOSMOS sample, Lilly et al. 2008, in preparation), will be presented in a forthcoming paper (Coppa et al., in preparation).

2. Description of zCOSMOS observations and data reduction

For an exhaustive discussion of the zCOSMOS survey design, in particular of the assembly of the input catalogues, the target selection, and the spectroscopic mask design, we address the reader to the survey presentation paper (Lilly et al., 2007).

The brighter part of zCOSMOS project consists of spectroscopic data of targets identified by means of a pure magnitude-limited selection $I_{AB} < 22.5$, as used in the CFRS (Lilly et al., 1995) and VVDS-wide surveys (Le Fèvre et al., 2005). This selection culls galaxies mainly in the redshift range $0.1 < z < 1.2$. A medium resolution grism ($R \sim 600$) has been used with a slit width of 1 arcsec, to achieve a velocity accuracy of ~ 100 kms^{-1}, and with one hour integrations to enable redshifts to be measured with a high success rate. The spectral range of observations is typically $5550 - 9650$ Å, which enables important spectroscopic diagnostic lines, centered on a rest-frame wavelength of approximately 4000Å, to be measured out to a redshift of about 1. The one hour total integration is acquired in five $720\,s$ exposures, between which the telescope was placed at different offset positions to complete an optimal sky subtraction, in a pattern of positions separated by one arcsec along the slit. The observations were executed during periods when the seeing was better than 1.2 arcsec. The first zCOSMOS-bright spectroscopic observations were completed in VLT Service Mode between April and June 2005. Eight sets of VIMOS mask observations were com-

pleted, which provided spectra of 1303 objects, corresponding to about 6% of the planned bright survey program. The data reduction was carried out using the *VIPGI* software, developed specifically for data acquired by VIMOS instrument (Scodeggio et al., 2005). Lilly et al. (2007) described the redshift determination procedures and the assignment of confidence classes to each measured redshift. The confidence in the redshift determination was indicated by a flag, whose values were: 4 (completely secure redshift); 3 (very secure redshift, but with a very marginal possibility of error); 2 (a likely redshift, but with a significant possibility of error); 1 (possible redshift); 0 (no redshift determination); and 9 (redshift based on a single strong emission line). The high quality of the photometric measurements for the COSMOS field and the corresponding photometric redshifts at $z < 1.2$ (Feldmann et al., 2006), implied that the photometric redshifts could be used to assess the spectroscopic redshift reliability of our zCOSMOS-bright spectra. To indicate the reliability of a redshift, we added a decimal place to its confidence flag: if the difference between the photometric and spectroscopic redshift, $|z_p - z_s|$, was less than $0.1 \times (1 + z_s)$, we added the decimal place=.5; otherwise, we added a decimal place=.1. In the following, we include in the spectroscopic "high quality" data set all the galaxy spectra with flag 3 and 4, and those with flag 2.5, which includes galaxy spectra with flag=2 confidence for which the photometric and spectroscopic redshifts are in good agreement. We exclude from the high quality data set galaxy spectra of flag 9, where the redshift could be determined using only one emission line; although this flag corresponds to significant detection of an emission line, the absence of other spectroscopic diagnostic lines implies that for many the continuum signal-to-noise ratio (hereafter S/N) could be rather low.

3. Spectral Analysis

3.1. Spectral Measurements

We performed spectral measurements for a total of 1130 galaxies (and 20 QSOs) observed during the first year of observations and for which a redshift had been determined. This set of extragalactic objects forms the analyzed 1*k* zCOSMOS-bright sample.

We measured the spectral quantities using semi-automatic procedures that were adaptations of the IRAF task `splot`. First, the continuum was fitted automatically to fixed wavelength intervals, although our procedures also enabled interactive adjustments of the continuum level to improve the line measurement in noisy spectra. Then, equivalent widths (EWs) and fluxes were measured by both applying a Gaussian-function fitting algorithm and direct integration of the continuum-subtracted line profiles. The fluxes measured by both techniques were in excellent agreement: for all emission lines, the two measurements agreed to within 25%, while the 1-σ dispersion of the difference distribution corresponded to only 11%. Figure 1 shows the distributions for principal spectroscopic line measurements for the 1*k*-sample. The equivalent widths are given in the rest-frame, and indicated by positive or negative values for emission or absorption lines, respectively. Errors in the measured equivalent widths were estimated by taking into account both the measured r.m.s. of the continuum close to the lines and the difference between the values derived by the two techniques. The median uncertainty in an individual EW is 0.7 Å, but it is worth noting that we did not account for the stellar absorption in the measurements of the Balmer emission lines, since in most cases the S/N of our spectra did not enable a simultaneous fit of both the absorption and emission components. We measured EWs and fluxes

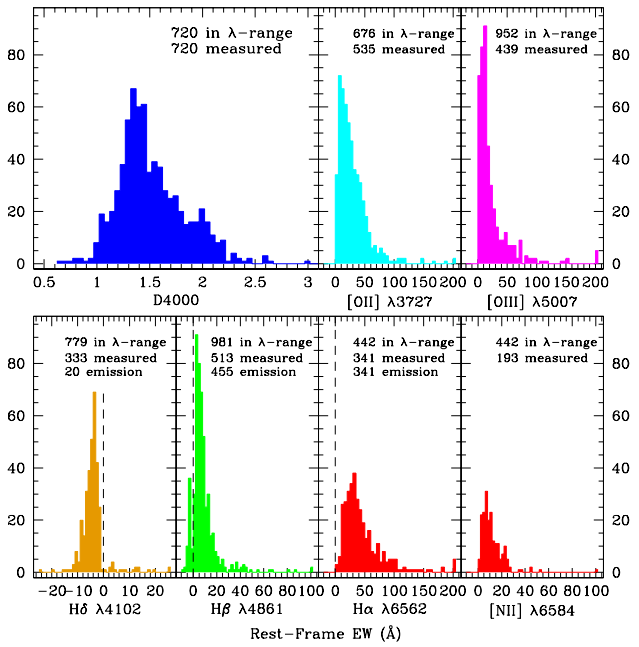


Fig. 1. Rest-frame measurement distributions of the analyzed spectral features, from top-left to bottom-right: *D*4000, and EW of the lines [OII]λ3727, [OIII]λ5007, Hδ, Hβ, Hα, and [NII]λ6584. In each panel, we indicate the number of galaxies for which the feature is within the spectral observed range and the number of measured lines.

for [OII]λ3727, Hδ, Hβ, [OIII]λ5007, Hα, and [NII]λ6584, as well as the strength of the 4000 Å break (*D*4000; Bruzual, 1983). The continuum fluxes were measured in fixed wavelength ranges, and our procedure computed the average using a sigma-clipping technique, to ensure that spikes, due to bad sky subtraction and/or to cosmic-ray residuals, did not affect significantly the measured values. Errors in the continuum fluxes were then computed from the standard deviation. We focused our analysis on EW measurements and flux ratios because the absolute spectrophotometry was not completely reliable due to the corrections for slit losses that had been applied to the spectra. This set of "semi-automatic" measurements was used, in addition, to test and calibrate the fully automatic measurement code PlateFit (Lamareille et al., 2006), which is being applied to larger zCOSMOS data sets.

In order to estimate our emission line detection limits, we measured the signal-to-noise ratio in the continuum adjacent to the lines. Figure 2 shows the relation between the S/N in the continuum and the observed equivalent widths of the measured emission lines in our sample: from this figure, it is clear that a correlation exists between the minimum detected EW and the continuum S/N. The lower envelope of the measured EWs (dotted line in Fig. 2) is well described by the curve

$$EW(detection\ limit) = \frac{SL * \Delta}{(S/N)_{cont}} \quad (1)$$

where Δ is the resolution element (in Å) of our spectra and SL is the significance level of the detectable line, expressed in terms of sigma of the continuum noise (Colless et al., 1990; Manning, 2002). On the basis of Fig. 2, we adopt a $SL(\sigma) = 3.5$. Measuring the S/N in the continuum of each galaxy spectra without a detectable emission line, we estimate the EW upper limits

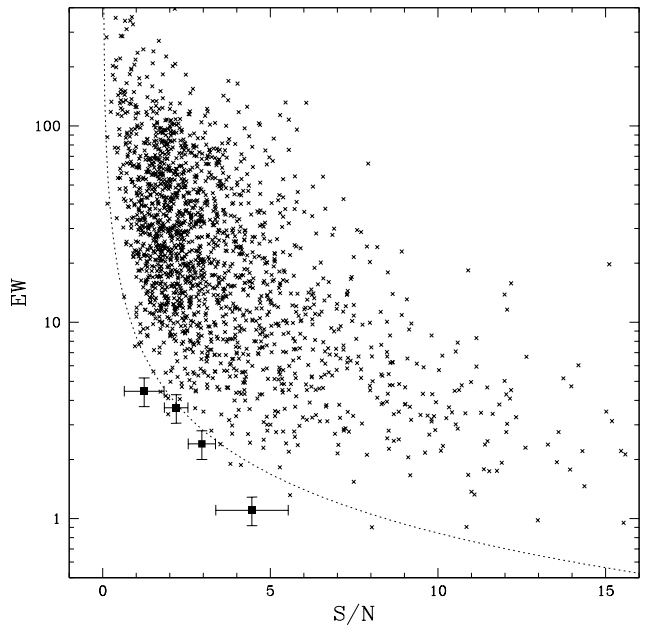


Fig. 2. Observed EWs of all the measured emission lines (see Fig. 1) versus the signal-to-noise ratio of the continuum close to the line; the lower envelope of the measured equivalent widths is fitted well by the dotted curve (see Eq. 1 in the text). The larger filled square symbols represent the [OII] EW values measured in composite spectra of galaxies that individually did not demonstrate a detectable emission line, grouped in four equally populated bins according to their continuum S/N; the line EWs have been measured in the composite spectra shifted to mean redshift of the corresponding galaxy group. The horizontal error bars indicate the range of S/N included in each bin, whereas the vertical error bars show the variation in the observed EW if the composite spectra were moved to the extremes of the redshift range.

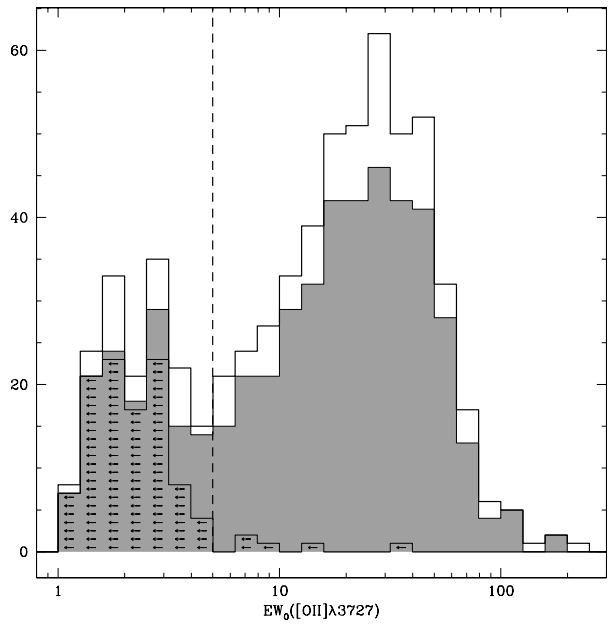


Fig. 3. Distribution of the rest-frame [OII] EWs for the zCOSMOS galaxy 1*k*-sample. The gray histogram represents the parameter distribution for galaxies included in the high-quality data set, with leftward arrows indicating the upper limits calculated using Eq. 1; the thin empty histogram is for the whole sample.

(using Eq. 1). The robustness of this technique in estimating the line upper limits is demonstrated by the detection of the emission lines (in particular [OII]λ3727) in composite spectra of galaxies without a detectable emission line. We grouped 141 single spectra in four equally populated bins according to their continuum S/N, and all the measured [OII] EWs lie below the curve calculated using the above equation (large squares in Fig. 2).

3.2. Galaxy Spectral Classification

Following Mignoli et al. (2005), we applied to the zCOSMOS-bright galaxy data set the straightforward spectral classification scheme adopted for the *K*20 survey (Cimatti et al., 2002), which uses the equivalent width of the [OII]λ3727 line and the 4000 Å break index to define two main spectral classes: *red quiescent galaxies*, which show a large *D*4000 value and a faint, if not undetected, [OII] emission line; and *blue star-forming galaxies*, with small *D*4000 and intense emission lines. This spectral classification scheme naturally arises from the intrinsic bimodal nature of galaxy physical properties that has been observed in the colour distribution (Balogh et al., 2004b; Bell et al., 2004) and mean spectroscopic indices (Kauffmann et al., 2003; Franzetti et al., 2007). In Fig. 3, the distribution of the rest-frame [OII] equivalent widths is shown for the zCOSMOS galaxy 1*k*-sample. A clear bimodality is evident in the EW$_0$([OII]) distribution, especially if we consider that the histogram with leftward arrows represents the upper limits to line measurements. On the basis of this behaviour, we separate the galaxy population into two classes, strong and weak line emitters, divided by an EW$_0$([OII])=5Å. With this threshold, almost all the objects with undetected emission lines are included in the weak emission line galaxy group. Most galaxies with high EW that are not included in the high-quality sample are flag=9 objects (see end of Sect. 2).

Looking at Fig. 4, a couple of comments can be made. First, the "low-density" region in the leftward corner of the classification plane is populated mainly by poor-quality flagged objects (indicated by crosses in the figure), confirming both the doubtful nature of their redshift identification and the efficiency of the spectral classification scheme. The galaxies in this region of the plane are not spectroscopically classified. Furthermore, when applied to the high-ranked zCOSMOS galaxies, the classification scheme demonstrates its efficiency: only four objects fall marginally in the leftward region of the plot, whereas the intermediate class (red emission line galaxies) constitutes only 4% of the sample. Interestingly, the few (broad line) active nuclei observed in the useful redshift range are quite segregated in the classification plane (see the encircled symbols in Fig. 4), having very blue continuum but relatively faint [OII] emission lines (<10Å, Forster et al., 2001).

Figure 4 shows the resulting spectral classification plane. Due to the high quality of zCOSMOS spectroscopic data, higher than in the *K*20 survey, we are able to appreciate how most of the galaxies with intense emission lines occupy a narrow region in the *D*4000-[OII] plane. We performed an iterative linear least squares fit with σ-clipping, to define and delimitate the locus

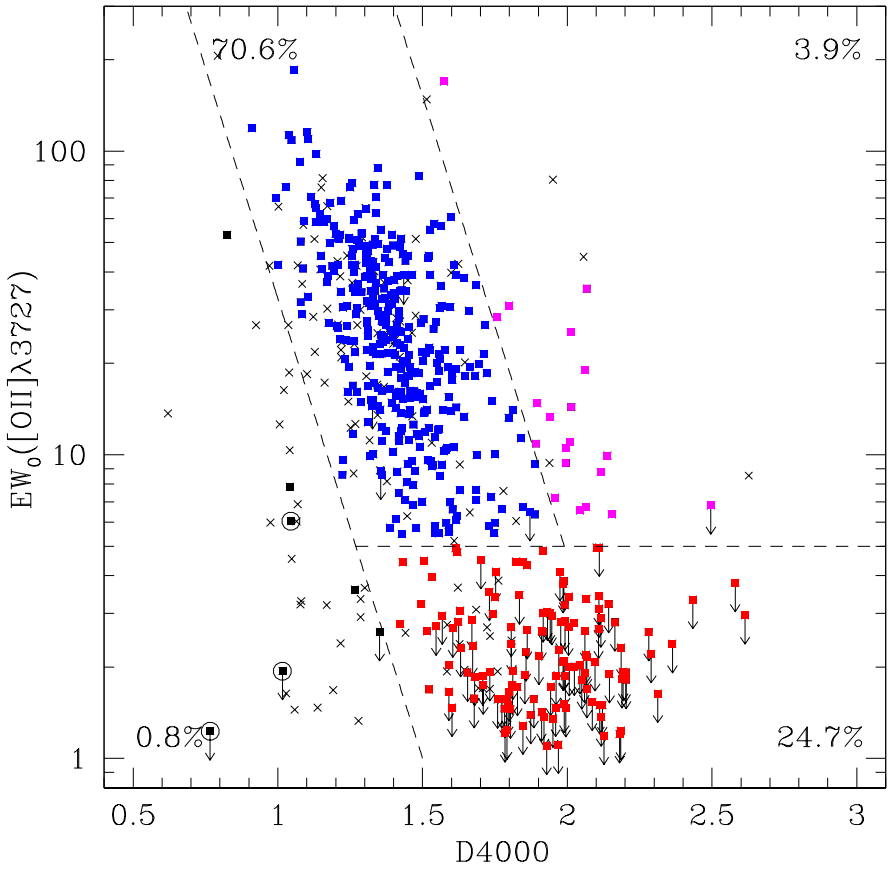


Fig. 4. The classification plane for the 1k zCOSMOS galaxies; using the rest-frame [OII]λ3727 EW and $D4000$, we define three main classes: *red quiescent galaxies* (lower right region), *blue emission-line galaxies* (upper left region) and the *intermediate galaxies*, which show emission lines but a large value of $D4000$. In the figure, we plot all classifiable galaxies (with $z \sim 0.45 \div 1.25$), with different symbols following the redshift quality ranks (crosses for the low-quality spectra, filled squares for the high-quality ones). Broad line objects (quasars) are encircled in figure. The dashed lines represent the boundaries of the adopted classification scheme following Eq. 2. The percentage of high quality galaxies falling in each classification regions are labelled at plot corners.

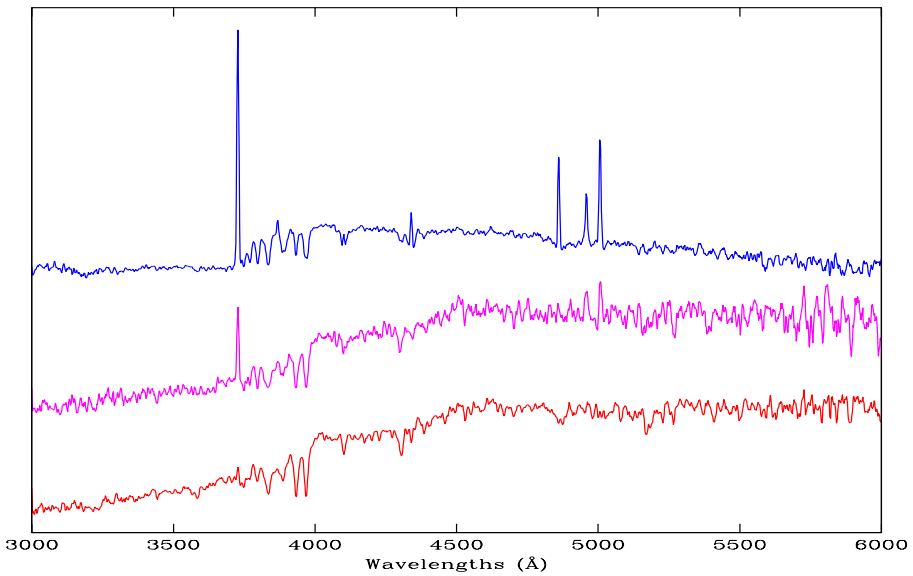


Fig. 5. Composite spectra of the three main galaxy classes as defined in Fig. 4. From bottom to top: 126 red quiescent, 20 intermediate and 361 blue star-forming galaxies contribute to the averages.

of these objects (see diagonal dashed lines in Fig. 4). The final criterion adopted to define the blue emission line galaxies was

$$EW_0([\mathrm{OII}]) \geq 5\text{Å},$$
$$1.50 \leq D4000 + 0.33 \times \log\left(EW_0([\mathrm{OII}])\right) \leq 2.22 \quad (2)$$

A relationship between the $D4000$ and the [OII] equivalent width was expected, since both features are related to the galaxy star-formation history, either the most recent one ($EW_0([\mathrm{OII}])$) or its integral over time ($D4000$). It is particularly encouraging that, by projecting our linear fit in the $D4000$-specific SFR plane, with the simple assumption of constant mass-to-luminosity ratio, we reproduce almost exactly the mode of the SDSS data distribution presented in Fig. 11 of Brinchmann et al. (2004).

It is worth keeping in mind that the observed spectral range enables us to apply this spectral classification scheme only to galaxies of sufficiently high redshift to include the [OII]–$D4000$ region, i.e. the redshift range $z \sim 0.45-1.25$. Within this redshift range, 631 galaxies were classified, of which 511 belong to the high-quality sample on the basis of the assigned redshift flag. More than 80% of the spectroscopically classified zCOSMOS galaxies belong to the two previously defined classes: *red quiescent galaxies* and *blue star-forming galaxies*. A third group of objects, which have emission lines but a red stellar continuum (as implied by their high value of $D4000$), constitutes what we refer to as the intermediate class of galaxies. Interestingly, 20% of these objects show some sign of nuclear activity: three of the twenty galaxies in this class are classified as Seyfert 2 galaxies (Bongiorno et al., in preparation) on the basis of the diagnostic diagrams of Baldwin et al. (1981), and one additional galaxy has an X-ray counterpart (Brusa et al., 2007). In contrast, the fraction of the blue star-forming galaxy population that are candidate AGN is only 2%, i.e. 7 out of 361 galaxies.

Composite spectra for each galaxy class were generated by averaging all spectra included in that class. To create the composites, each spectrum was shifted to the rest-frame according to its redshift (with a 1.5 Å rest-frame bin[1]) and normalized in the 4000-4500 Å wavelength range, which was always present in the observed spectroscopic window. An identical weight was assigned to each individual spectrum, to avoid biasing the final composite towards the brightest galaxies. Finally, all spectra belonging to a particular spectroscopic class were stacked. In Fig. 5, the average spectra of the three main spectroscopic classes are plotted. The continuum in the composite of the emission line galaxies with red $D4000$ is largely indistinguishable from that of the purely passive galaxies composite. Therefore, this class of intermediate objects should consist mainly of galaxies undergoing a modest star-formation episode, rather than of heavily reddened star-forming galaxies. The presence of the [OIII] emission doublet, with no evidence of $H\beta$ in emission, in the composite of intermediate objects could indicate some nuclear activity (i.e. type II AGNs) contamination in this galaxy class, as already noted above (see also Yan et al., 2006).

4. Photometric colours of galaxy spectral classes

The bimodality in the galaxy spectroscopic index measurements identified above may be naturally linked to the colour bimodality observed widely in the galaxy population. We therefore compare the observed colours and spectral classification of galaxies that belong to the zCOSMOS-bright 1k-sample.

The photometric observations of the COSMOS field that we use in our study include optical (B_J, g^+, V_J, r^+, i^+, and z^+ data acquired using SuprimeCam at the Subaru Telescope, u^*-band data with the Canada–France–Hawaii Telescope and i_{814} images with ACS/HST) and near-Infrared (K_s-band data acquired using the Cerro Tololo International Observatory and Kitt Peak National Observatory telescopes) wavelengths. Details of the ground-based observations and data reduction are presented in Capak et al. (2007) and Taniguchi et al. (2007). The reduced images in all bands were PSF-matched by Gaussian convolution with a final FWHM corresponding to the seeing in the K_s-band (1.5″); the multi-band photometry catalog was then generated using SExtractor (Bertin & Arnouts, 1996). First, the total (SExtractor magauto) and fixed-aperture (3″–diameter) magnitudes were measured on the detection image (i-band), allowing the estimate of the aperture correction for each galaxy. This correction was applied subsequently to aperture magnitudes measured in the other optical/near-IR bands. Details of the photometry, star/galaxy separation, and catalog construction were provided by Capak et al. (2007).

We analyzed different colours from the photometric catalog and attempted to identify a separation in photometric space between the above defined spectral galaxy classes. The $B-z$ colour, in addition to both $B-K$ and $u-i$, appears to provide the most effective way of separating red quiescent and blue star-forming galaxies. In Fig. 6, we illustrate, in the $B-z$ distribution histograms (upper panel; cyan histogram for blue star-forming, red histogram for quiescent galaxies, both with and without emission lines), the good separation between the colour distribution of the different spectral classes, although with some overlap for $2 < B-z < 3$. We verified whether the slit aperture effects would bias the comparison between the observed colours and spectral classification: the slit corrections, estimated on the basis of the difference between the integrated magnitudes computed from the flux-calibrated spectra and the I-band photometric data, do not show any trend both with the magnitude and $B-z$ colour in the analyzed sample.

The correlation between colour and spectral classification becomes even tighter when we consider galaxy redshifts. The $B-z$ versus redshift plot (lower panel; cyan and red squares for star-forming and quiescent galaxies, respectively, magenta crosses for intermediate ones) exhibits a clear segregation between the galaxy classes. To divide effectively the two galaxy populations, we adopted the $B-z$ versus redshift evolutionary track of a template spectrum from the Coleman, Wu & Weedman Extended set (Coleman, Wu & Weedman, 1980; Sawicki et al., 1997) with properties corresponding most closely to those dividing the two populations. The chosen template had the optical colours (Fukugita et al., 1995) and spectral appearance (Kennicutt, 1992) of an Sab galaxy. Also in local galaxy samples (i.e. The Revised Shapley-Ames Catalog of Galaxies; van den Bergh, 2007), the transition between blue and red galaxies occurs at the Hubble type Sab/Sb.

The lower panel of Fig. 6 shows that almost all of the small number of discordant galaxies (blue quiescent and red star-forming) fall close to the separation track in the colour classification plane, confirming the agreement between the spectral and photometric classification. Moreover, galaxies of the intermediate spectral class (red $D4000$ with emission lines, magenta crosses in Fig. 6) have a colour distribution similar to that of quiescent galaxies, in agreement with the observed similarity of the stellar continuum in the composite spectra noted above (Fig. 5).

[1] at the median redshift of the analyzed galaxy sample ($z = 0.724$), a rest-frame bin of 1.5 Å matches the pixel size used in the spectroscopic observations.

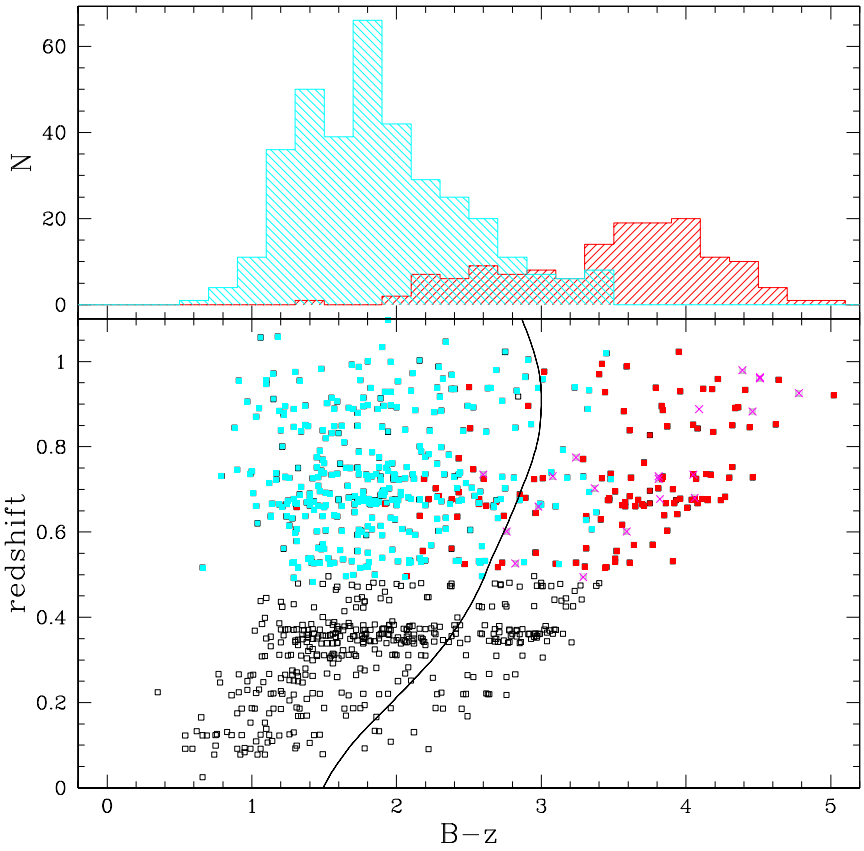


Fig. 6. Upper Panel: observed $B-z$ colour distribution of the galaxies belonging to zCOSMOS-bright $1k$-sample with $0.45 \leq z \leq 1.2$; cyan histogram for blue star-forming, red histogram for quiescent galaxies, both with and without emission lines. Lower Panel: $B-z$ versus redshift plot for the whole high quality sample; cyan and red squares for star-forming and quiescent galaxies respectively, magenta crosses for intermediate ones). We divide the two galaxy populations using as discriminator the $B-z$ track of the Sab template from the Coleman Wu & Weedman Extended set (solid line in figure; Sawicki et al. (1997)).

By merging these two spectral classes and using the track of the Sab-template to separate the photometrically "blue" and "red" galaxies, we compiled a 2×2 contingency table for the high quality sample (Table 1), useful in performing a statistical analysis of the relationship between the spectral and photometric classification. To quantify the degree of correlation between the two classification schemes, we computed Pearson's linear correlation coefficient for the data presented in Table 1: the two classifications are well correlated, as indicated by a Pearson coefficient of 0.77.

Table 1. Numbers of galaxies in the spectroscopic and photometric classes

	Spectral classification		
$B-z$	Quiescent	Star-forming	TOTAL
Red	119	20	139
Blue	27	335	362
TOTAL	146	355	501

In the following, we summarize how the different galaxy populations inhabit the colour versus spectral classification plane:

- 82% of objects classified as "quiescent" from spectra are red;
- 94% of objects classified as "star-forming" from spectra are blue;
- 86% of objects with red colours are "quiescent" from the spectra;
- 93% of objects with blue colours are "star-forming" from the spectra.
- The fraction of outliers is ~9% (47/501).

The correspondence between the two classifications is not optimal for the 18% quiescent galaxies that show bluish colours. We investigated the nature of these objects by studying their composite spectrum. The continuum in the composite of blue quiescent galaxies is largely indistinguishable from that of the red, quiescent galaxies, but the spectrum shows a moderate [OII] emission line ($EW_0 = 4.4$Å) and a strong $H\delta$ in absorption ($EW_0 = -3.8$Å). The presence of these two spectral features represents star formation activity, which could also explain the bluish colours of this class of galaxy. The rest-frame equivalent width of [OII], measured in the composite spectrum, is below the cut adopted for the spectral classification (EW_0([OII]) > 5Å), and only one of the 27 blue quiescent galaxies is spectroscopically classified as intermediate. Therefore, it is more reasonable to consider these objects as being galaxies in-between the two main spectral classes, rather than galaxies of extremely

discordant spectral and colour properties. Indeed, about 30% of these galaxies can be spectroscopically classified as post-starburst galaxies and constitute the 64% of the 1k sample of post-starburst galaxies (7/11; Vergani et al., in preparation).

The good agreement between the classification from spectral data (quiescent/star-forming galaxies) and that based on colours (red/blue galaxies) is achieved within the relatively bright (I_{AB} < 22.5) zCOSMOS sample; using the deeper (I_{AB} < 24.0) VVDS survey, Franzetti et al. (2007) demonstrated that the incidence of red star-forming or blue quiescent galaxies appear to increase when studying fainter galaxy samples.

5. ACS Morphology of galaxy spectral classes

The HST/ACS imaging is an integral component of the COSMOS survey, providing very high sensitivity and high resolution imaging over a large field of view. These space-based images yield resolved morphologies for several hundreds of thousands galaxies, and the zCOSMOS-bright survey magnitude limit (I_{AB} < 22.5) is matched with the I-band ACS depth to allow classical bulge-disk decomposition. The COSMOS survey is a natural "battlefield" for competing morphological classification schemes. Among all the possible and equally good techniques implemented by the various teams within the COSMOS collaboration, we selected as our morphological classification tool the *Zurich Estimator of Structural Types* (ZEST; Scarlata et al., 2007a). We adopted this approach mainly because $ZEST$ classifies galaxy types by applying a variety of non-parametric techniques that measure physical parameters directly on the ACS images in a way similar to how we classify galaxies in terms of both spectroscopic and optical colour data.

In brief, $ZEST$ quantitatively describes the galaxy structure using three variables (PC1; PC2; PC3), obtained by performing a principal component analysis (PCA) in the five-dimensional parameter space defined by asymmetry (A), concentration (C), Gini coefficient (G), the 2nd-order moment of the brightest 20% of galaxy pixels (M20), and the ellipticity of the light distribution (ϵ). The morphological classification is performed in the PC1-PC2-PC3 space by linking a (dominant) morphological class to different regions in the PC-space. Finally, $ZEST$ assigns each analyzed object to a straightforward morphological Type (= 1 for early-type galaxies, = 2 for disk galaxies and = 3 for irregular galaxies). Furthermore, a "bulgeness" parameter (from 0 for bulge-dominated galaxies to 3 for bulge-less disks) is also assigned to each galaxy classified as Type 2 (Scarlata et al., 2007a), following the median value of the Sersic indices distribution of galaxies clustered in the PC-space. The Sersic indices were computed by Sargent et al. (2007).

We compare the spectral classification with the morphological characterization assigned by $ZEST$ in Fig. 7, where the histograms represent the frequency distributions of the morphological types for the three main spectroscopic classes. This figure illustrates a fairly good correlation between the spectral and the morphological classification, represented by a gradual increase in the fraction of star-forming galaxies towards morphological late-types, and, similarly, an increase in spectroscopic quiescent galaxies towards the morphological early-types.

A more instructive way to look at the correspondence between the morphological and spectral classifications is presented in Fig. 8, which shows the distribution of the morphological types in our spectral classification plane. Following the morphological characterization, we divided the galaxies into: (*i*) "spheroids", a class including both the pure ellipticals

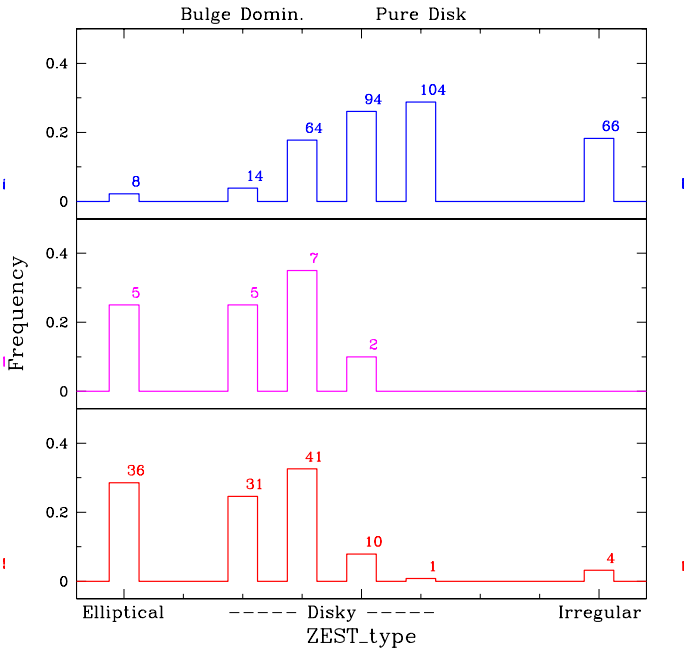


Fig. 7. Frequency distributions of $ZEST$ morphological types for the spectroscopic blue emission line galaxies (top histogram), the spectroscopic intermediate galaxies (i.e. galaxies which show red continuum with emission lines; middle histogram), and the quiescent galaxies (bottom histogram). The four central bins represent the most-populated $ZEST$ class of disk galaxies, further splitted on the basis of the "bulgeness" parameter. The numbers on top of the bars indicate the number of galaxies in each bin.

($ZEST$-type = 1) and the bulge-dominated galaxies ($ZEST$-type = 2 with bulgeness parameter = 0)[2]; (*ii*) "morphologically-mixed" objects, disky ($ZEST$-type = 2) galaxies with intermediate bulgeness parameter (= 1); (*iii*) "disk-dominated" galaxies with $ZEST$-type = 2 and bulgeness parameter ≥ 2; and (*iv*) "irregulars", with $ZEST$-type = 3. The four panels of Fig. 8 demonstrate that all but one of these morphologically defined galaxy types appear to occupy the regions expected based on their spectral classification. More than 90% of the morphological ellipticals are quiescent from the spectra, as well as a large fraction (82%) of the spheroids. Also, more than 90% of the disk-dominated and irregular galaxies have blue emission line spectra. Only the morphologically mixed objects (i.e. disk galaxies with intermediate B/T parameters) are spread all over the spectral classification plane. Table 2 shows the distribution of $ZEST$ types in the 1k-galaxy sample as a function of their spectroscopic class.

The application of a 2 × 2 contingency table, as a statistical test of correspondence between the spectral and morphological classifications, is not a straightforward exercise in this case, since it is difficult to assign objects with $ZEST$-type = 2.1 to an early- or late- galaxy type.

Bailin & Harris (2008) discovered a similar population of morphologically intermediate SDSS galaxies, finding that inclination effects play an important role in their classification. Nevertheless, both a visual inspection of the ACS snapshots and a statistical analysis of the asymmetry and ellipticity parame-

[2] the inclusion of the bulge-dominated disk galaxies into the same class as pure ellipticals was already proposed by Scarlata et al. (2007b)

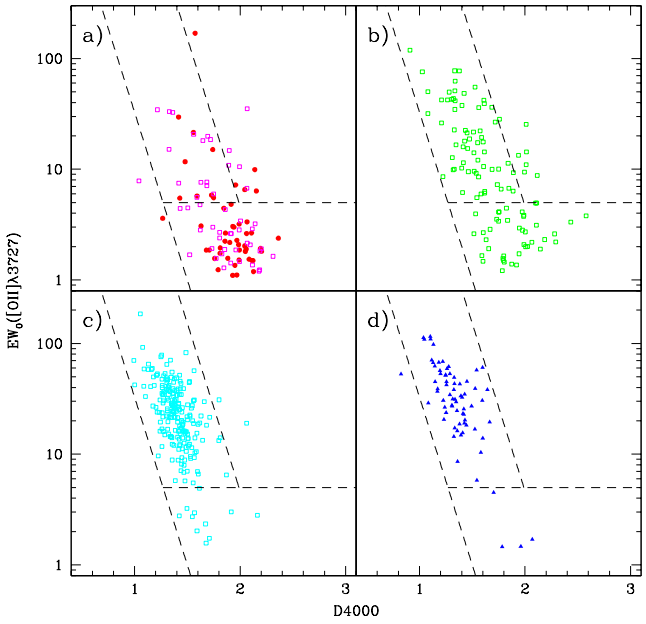


Fig. 8. Distributions of different morphological groups in our spectral classification plane. Panel a): Spheroidal galaxies, including both pure ellipticals ($ZEST$-type = 1; filled circles) and bulge-dominated galaxies ($ZEST$-type = 2.0; empty squares). Panel b): disky galaxies with intermediate bulgeness parameter ($ZEST$-type = 2.1; empty squares). Panel c): "disk-dominated" galaxies ($ZEST$-type = 2.2 and = 2.3; empty squares). Panel d): Irregular galaxies ($ZEST$-type = 3; filled triangles). In all the four panels, the dashed lines indicate the spectral class boundaries.

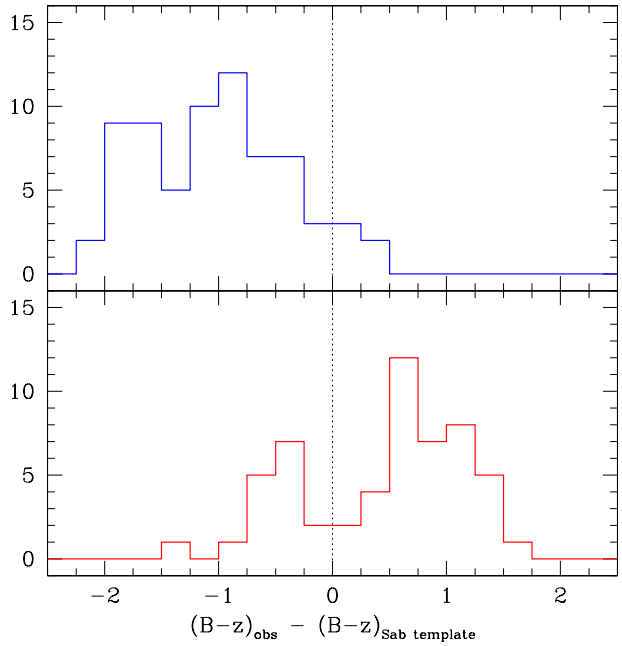


Fig. 9. The distribution of the differences between the observed $(B-Z)$ colour of the Type = 2.1 galaxies and the colour, at the redshift of each galaxy, of the Sab template adopted to photometrically separate the blue and red populations in Fig. 6. In the upper panel, the galaxies spectroscopically classified as star-forming; in the lower panel, the galaxies spectroscopically classified as quiescent.

Table 2. Numbers of galaxies in the spectroscopic and ZEST classes

$ZEST$-type	Spectral classification		
	Quiescent	Star-forming	TOTAL
1.0-2.0	76	24	100
2.1	55	70	125
2.2-3.0	11	256	267
TOTAL	142	350	492

ters do not suggest the presence of an inclination bias in the zCOSMOS galaxies with $ZEST$-type = 2.1. This intermediate morphological class is plausibly composed of galaxies spanning a wide range of bulge-to-disk ratios and $ZEST$ alone is unable to identify a dominant component in their visual morphology. We decided to fully utilize the classification cube potentialities, including the photometric colours, in the analysis of this intermediate morphological class. Figure 9 shows the colour distribution of $ZEST$-type = 2.1 galaxies, divided following the spectral classification. The upper panel shows the distribution of the differences between the observed $(B-z)$ colour and the colour, at the same redshift of each galaxy, of the Sab template adopted to separate the blue and red populations in the previous section, for galaxies spectroscopically classified as star-forming; the lower panel shows the same colour difference for the Type = 2.1 galaxies spectroscopically classified as quiescent. The figure clearly shows that galaxies with $ZEST$-type = 2.1 have $B-z$ colours largely in agreement with their spectral classification: 93% (65/70) of the $ZEST$ Type = 2.1 classified as "star-forming" from the spectra have blue colours, whereas 71% (40/55) of the $ZEST$ Type = 2.1 classified as "quiescent" from the spectra have red colours. Interestingly, the latter galaxy class exhibits a bimodal colour distribution, which is separated well by the colour track of the Sab template. We investigated the average properties of the two classes of red and blue quiescent galaxies with intermediate ZEST morphology by means of the analysis of their composite spectra: the stellar continuum appears similar in the two composites, resembling that of the normal quiescent galaxies (see Fig. 5), even if the average spectrum of the blue quiescent class is of low signal-to-noise ratio because of the small number of coadded galaxy spectra. The main difference is the presence of emission lines in the blue quiescent composite (with EW([OII])~5Å), while emission lines are undetected in the red quiescent composite. However, the careful analysis of single galaxy sub-classes is beyond the scope of this paper, and are the subject of a forthcoming paper in which the properties of these galaxy classes will be revisited using a larger zCOSMOS data set.

Table 3. Numbers of galaxies in the spectroscopic and morphological classes

Morph+$(B-z)$	Spectral classification		
	Quiescent	Star-forming	TOTAL
Spheroids	115	29	144
Disk/Irr	27	321	348
TOTAL	142	350	492

We therefore separated the galaxies of this morphological class by colour, by assigning the red-coloured Type 2.1 galaxies to a Spheroid class and the blue-coloured Type 2.1 galaxies to a Disk/Irregulars category. Following this recipe, we derived a 2×2 contingency table (Table 3), which provided a clear indication of the correlation between the two classifications (Pearson correlation coefficient= 0.73).

6. The galaxy classification cube

It is evident from the previous sections that strong correlations are present between the spectral classification and both the colour and morphological properties of the zCOSMOS-bright galaxies. In this section, we merge these classifications into a three-dimensional characterization, the galaxy classification cube. We include in our analysis all galaxies with $0.45 \leq z \leq 1.25$ [3] and complete photometric and morphological information. The full sample includes 577 galaxies, of which 487 (84%) belong to the high-quality spectroscopic sample on the basis of the assigned redshift flag.

A three-digit code was then assigned to each galaxy of the sample, such that each digit represented one of the three classifications (spectral, photometric, and morphological, respectively). Each digit can assume a bitwise value. This corresponds to 1, if the galaxy was spectroscopically classified as quiescent, had red $B-z$ colour, or its morphology was dominated by the bulge component. Alternatively, we assigned a digit value of 2 if the galaxy was spectroscopically star-forming, had blue $B-z$ colour or showed a disky or irregular morphology.

We recall two caveats related to both the procedure we adopted to separate galaxies into one of the two classes, and the presence of galaxies that deviate from the bimodal trends in properties (quiescent/star-forming, red/blue, bulge-dominated/disk-dominated). First, a galaxy spectrum with emission lines but a red stellar continuum (implied by a relatively high value of $D4000$) was classified spectroscopically as quiescent because their global properties indicated that they were probably ellipticals experiencing a modest star-formation episode or including a faint/obscured AGN. Secondly, we used the $B-z$ colour to determine a more robust separation of the galaxies included by ZEST in the intermediate class ($ZEST$ Type = 2.1).

Table 4. The Classification Cube: galaxy counts and class percentages

class-code s-c-m	High-Q. Sample N	(%)	All Galaxies N	(%)
2-2-2	311	(63.9)	374	(64.8)
1-1-1	105	(21.6)	113	(19.6)
1-2-2	18	(3.7)	26	(4.5)
2-1-1	13	(2.7)	17	(2.9)
2-1-2	7	(1.4)	8	(1.4)
1-2-1	9	(1.8)	11	(1.9)
2-2-1	15	(3.1)	17	(2.9)
1-1-2	9	(1.8)	11	(1.9)
TOTAL	487	(100)	577	(100)

[3] since the features adopted for spectral classification ($D4000$ and EW([OII])) can be seen in the zCOSMOS-bright spectra only within this redshift range

In Table 4, numbers and percentages of objects belonging to each cell of the classification cube are presented, using the three-digit code to identify the galaxy groups. The numbers for both the high-quality and the full sample are listed, and although all the single classification definitions were determined by using the high-quality sample, the percentages of galaxies included in each group vary only slightly between the two different samples. The main result emerging from the 3D analysis of the optical properties of the zCOSMOS-bright galaxies is that a large fraction of them shows a fully concordant classification: 85.5% (84.4%) of the analyzed galaxies in the high-quality (full) sample can be assigned consistently to the red or blue branch of the bimodal distribution using both a spectral, photometric, and morphological criterion. Due to the redshift constraints imposed by the spectral classification, we cannot explore a very large redshift domain. However, we divided the useful redshift range into two bins, so that each bin contained a similar number of objects: in the low-z range ($0.45 \leq z \leq 0.73$) 83.4% of the galaxies shows a fully concordant classification, while in the high-redshift range ($0.73 \leq z \leq 1.25$) this percentage slightly grows to 85.5%. We conclude that the fraction of galaxies for which the three classification schemes are in agreement remains constant (within our statistical errors) for the entire redshift range covered by our analysis.

7. Conclusion

We have presented a classification scheme for galaxies observed by the 1k zCOSMOS-bright sample, developed using spectral, colour, and morphological information. Since the spectral classification that we adopted is based on measurements of the [OII] and $D4000$ features, and given the wavelength range of the zCOSMOS spectra, we applied this classification scheme to galaxies in the redshift range $0.45 \leq z \leq 1.25$. We demonstrated that the adopted spectral classification is an effective way of separating galaxies into two main classes, due to the high quality of the zCOSMOS data.

We have found that an excellent correlation exists between the classification from spectral data (quiescent/star-forming galaxies) and that based on colours (red/blue galaxies), and that a similarly good correlation exists between the classification based on spectral data and that based on morphological analysis (early-/late-type galaxies) only if we complement the morphological classification with additional colour information. The "outliers" in this simple 2-way analysis of different classification methods (i.e. spectra versus colours and spectra versus morphology) are quiescent galaxies (high $D4000$ value) with emission lines (about 4% of the total sample of galaxies) and morphologically intermediate galaxies (about 20% of the total sample of galaxies) that consists of both blue/star-forming and red/quiescent galaxies. These are the morphologically-classified galaxies that require additional colour information to ensure good agreement between the classification of schemes using both spectroscopic and morphological data.

Finally, analyzing the distribution of all galaxies in a 3D-classification cube, based on the three different classification methods, we have found that for about 85% of the galaxies there is complete agreement between the classifications (i.e. quiescent, red, ellipticals or bulge-dominated galaxies ($\sim$ 20%) or star-forming, blue, disk-dominated galaxies ($\sim$ 65%)). If additional colour information was not used for the $ZEST$-type = 2.1 galaxies (i.e. by assigning all of them to the spheroid- or to the disk-galaxies), the percentage of fully concordant classifications would decrease to about 75%.

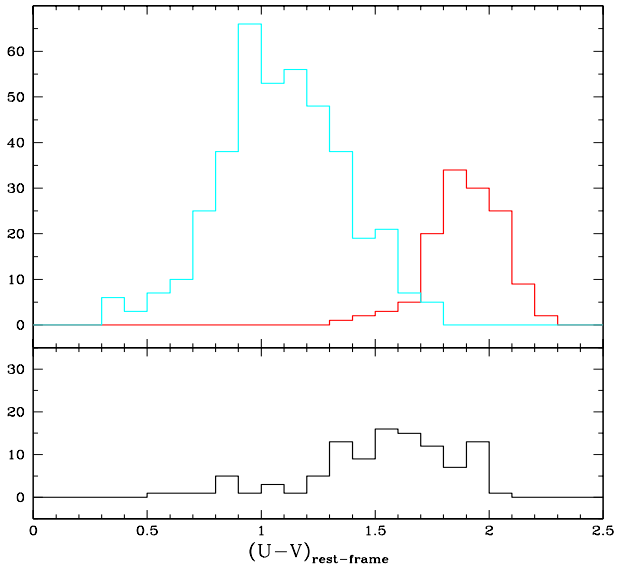


Fig. 10. Classification cube and rest-frame $U - V$ colour of the 1k zCOSMOS-bright data set. The upper panel shows the rest-frame colour distributions of galaxies with fully concordant classification, the blue histogram representing the star-forming, blue, disk-dominated galaxies, whilst the red histogram is for the quiescent, red, ellipticals or bulge-dominated galaxies. The lower panel shows the rest-frame colour distribution for the outliers, i.e. galaxies which do not present the same behaviour in all the three classifications.

The correspondence between the classification cube and classical representation of galaxy bimodality, which uses the rest-frame $U - V$ colours[4], is shown in Fig. 10. In the upper panel, as expected, the rest-frame $U - V$ colour distributions of the two galaxy groups with fully concordant classifications are separated well and reproduce the bimodality. Perhaps more interesting is the distribution of outliers in the lower panel, which is centered in-between the two branches of the galaxy bimodality, in the so-called 'green valley', the relatively sparse region between the blue cloud of star-forming galaxies, and the red sequence of quiescent ones.

The results presented in this paper demonstrate the potential of the data set provided by the COSMOS/zCOSMOS survey for investigating the nature of the observed relationships between galaxy properties and highlight fundamental aspects of the galaxy population. The main conclusion of this work is that the bimodality is a prevalent feature of the galaxy population, at least out to $z \sim 1$, in three critical parameters describing galaxy physical properties: morphological, colour, and spectroscopic diagnostic line data. More detailed analysis of the properties of both a wider sample of galaxies and outliers in this 3D-classification cube, based on an analysis of the larger 10K zCOSMOS-bright sample, will be presented elsewhere.

Acknowledgements. This work was partially supported by INAF under PRIN-2006/1.06.10.08 and by ASI under grant ASI/COFIS I/016/07/0.

References

Bailin, J. & Harris, W.E. 2008, ApJ, 681, 225
Baldwin, J.A., Phillips, M.M. & Terlevich R., PASP, 93, 5
Balogh, M.L., Eke, V.; Miller, C., et al. 2004a, MNRAS, 348, 1355
Balogh, M.L., Baldry, I.K., Nichol, R., et al. 2004b, ApJ, 615, L101
Baldry, I.K., Glazebrook, K., Brinkmann, J., et al. 2004, ApJ, 600, 681
Ball, N.M., Loveday, J., Brunner, R.J., et al. 2006, MNRAS, 373, 845
Bell, E.F., Wolf, C., Meisenheimer, K., et al. 2004, ApJ, 608, 752
Bershady, M.A., Jangren, A. & Conselice, C. 2000, AJ, 119, 2645
Bertin, E. & Arnouts, S. 1996, A&AS, 117, 393
Brinchmann, J., Charlot, S., White, S.D.M. et al. 2004, MNRAS, 351, 1151
Brusa, M., Zamorani, G., Comastri, A., et al. 2007, ApJS, 172, 353
Bruzual, G. 1983, ApJ, 273, 105
Capak, P., Mobasher, B., Abraham, B., et al. 2007, ApJS, 172, 99
Cassata, P., Cimatti, A., Kurk, J., et al. 2008, A&A, 483, L39.
Cimatti, A., Mignoli, M., Daddi, e., et al. 2002, A&A, 392, 395
Cirasuolo, M., McLure, R.J., Dunlop, J.S., et al. 2007, MNRAS, 380, 585
Coleman, G.D., Wu, C.-C., & Weedman, D.W. 1980, ApJS, 43, 393
Colless, M., Ellis, R.S., Taylor, K. & Hook, R.N. 1990, MNRAS, 244, 408
Conselice C.J. 2006, MNRAS, 373, 1389
Drory N. & Fisher D.B. 2007, ApJ, 664, 640
Feldmann, R., Carollo, C.M., Porciani, C., et al. 2006, MNRAS, 372, 565
Fioc, M. & Rocca-Volmerange, B. 1999, A&A, 351, 869
Forster, K., Green, P.J., Aldcroft, T.L., et al. 2001, ApJS, 134, 35
Franzetti, P., Scodeggio, M., Garilli, B., et al. 2007, A&A, 465, 711
Fukugita, M., Shimasaku, K., & Ichikawa, T. 1995, PASP, 107, 945
Giallongo, E., Salimbeni, S., Menci, N. et al. 2005, ApJ, 622, 116
Ilbert, O., Tresse, L., Zucca, E. et al. 2005, A&A, 439, 863
Hubble, E. 1938, PASP, 50, 97
Humason, M.L 1936, ApJ, 83, 10
Kauffmann, G., Heckman, T.M., White, S.D.M., et al. 2003, MNRAS, 341, 33
Kennicutt R.C. 1992, ApJS, 79, 255
Le Fèvre, O., Vettolani, G., Garilli, B., et al. 2005, A&A, 439, 845
Lamareille, F., Contini, T., Le Borgne, et al. 2006, A&A, 448, 893
Lilly, S.J., Le Févre, O., Crampton, D., et al. 1995, ApJ, 455, 50
Lilly, S.J., Le Fèvre, O., Renzini, A., et al. 2007, ApJS, 172, 70
Manning, C.V. 2002, ApJ, 574, 599
Mignoli, M., Cimatti, A., Zamorani, G., et al. 2005, A&A, 437, 883
Sargent, M.T., Carollo, C.M., Lilly, S.J.; et al. 2007, ApJS, 172, 434
Sawicki J.J., Lin H., Yee H.K. C., 1997, AJ, 310, 1
Scarlata, C., Carollo, C.M., Lilly, S.J., et al. 2007a, ApJS, 172, 406
Scarlata, C., Carollo, C.M., Lilly, S.J., et al. 2007b, ApJS, 172, 494
Scodeggio, M., Franzetti, P., Garilli, B., et al. 2005, PASP, 117, 1284
Scoville, N., Abraham, R.G., Aussel, H., et al. 2007, ApJS, 172, 38
Strateva, I., Ivezić, Z.; Knapp, G.R., et al. 2001, AJ, 122, 1861
Taniguchi, Y., Scoville, N., Murayama, T., et al. 2007, ApJS, 172, 9
van den Bergh, S. 2007, AJ, 134, 1508
Wild, V., Peacock, J.A.. Lahav, O., et al. 2005, MNRAS, 356, 247
Yan, R., Newman, J.A., Faber, S.M., et al. 2006, ApJ, 648, 281

[4] the rest-frame colours were computed following the method developed by Ilbert et al. (2005)